# *De novo* design of phospho-tyrosine peptide binders

Magnus S Bauer*[1,2], Jason Z Zhang*[1,2], Kejia Wu*[1,2], Gyu Rie Lee*[1,2,3,8], Brian Coventry*[1,2,7], Kody A Klupt[1,2,4], Jiuhan Shi[1,2], Rafael I Brent[1,2], Xinting Li[1,2], Carolina Moller[1,2], Nicole Roullier[1,2], Dionne K Vafeados[1,2], Indrek Kalvet[1,2,7], Rebecca K Skotheim[1,2], Siyu Zhu[1,2], Amir Motmaen[1,2], Luca C Herrmann[1,2], Pascal Sturmfels[1,2], Doug Tischer[1,2], Han Raut Altae-Tran[1,2], David Juergens[1,2], Rohith Krishna[1,2], Woody Ahern[1,2], Jason Yim[1,2,5], Asim K Bera[1,2], Alex Kang[1,2], Emily Joyce[1,2], Andrew Lu[6], Lance Stewart[1,2], Frank DiMaio[1,2], David Baker[1,2,7,8]

*These authors contributed equally
[1]Department of Biochemistry, University of Washington, Seattle, WA 98195, USA
[2]Institute for Protein Design, University of Washington, Seattle, WA 98195, USA
[3]Department of Biological Sciences, Korea Advanced Institute of Science and Technology, Daejeon, South Korea
[4]Department of Biomedical and Molecular Sciences, Queen's University, Kingston, ON, Canada
[5]Computer Science and Artificial Intelligence Laboratory, Massachusetts Institute of Technology, Cambridge, MA 02139, USA
[6]Department of Biology and Biological Engineering, California Institute of Technology, Pasadena, CA 91125, USA
[7]Howard Hughes Medical Institute, University of Washington, Seattle, WA 98195, USA
[8]Corresponding authors

## ABSTRACT

Phosphorylation on tyrosine is a key step in many signaling pathways. Despite recent progress in *de novo* design of protein binders, there are no current methods for designing binders that recognize phosphorylated proteins and peptides; this is a challenging problem as phosphate groups are highly charged, and phosphorylation often occurs within unstructured regions. Here we introduce RoseTTAFold Diffusion 2 for Molecular Interfaces (RFD2-MI), a deep generative framework for the design of binders for protein, ligand, and covalently modified protein targets. We demonstrate the power and versatility of this method by designing binders for four critical phosphotyrosine sites on three clinically relevant targets: Cluster of Differentiation 3 (CD3ε), Epidermal Growth Factor Receptor (EGFR) and Insulin Receptor (INSR). Experimental characterization shows that the designs bind their phospho-tyrosine containing targets with affinities comparable to native binding sites and have negligible binding to non-phosphorylated targets or phosphopeptides with different sequences. X-ray crystal structures of generated binders to CD3ε and EGFR are very close to the design models, demonstrating the accuracy of the design approach. RFD2-MI provides a generalizable all-atom diffusion framework for probing and modulating phosphorylation-dependent signaling, and more generally, for developing research tools and targeted therapeutics against post-translationally modified proteins.

## INTRODUCTION

Phosphorylation is one of the most critical post-translational modifications (PTMs) in cell signaling and other cellular processes. To probe and modulate these phosphorylations, phosphorylation-specific binding reagents are needed, yet current options are limited. Antibodies, the most commonly used class of binders, often fail to distinguish between closely related phosphosites (1–3), require long development times, and are constrained by a single scaffold architecture that limits the diversity of interaction surfaces. Directed evolution strategies using nature-derived domains that bind to phosphorylations like Src Homology 2 (SH2) or WW domains can improve general phospho-residue binding (e.g. phosphotyrosines (pY), phosphothreonines or phosphoserines), but lack the ability to discriminate between sequences flanking the phosphorylation site (4–7). This limitation is especially problematic for disordered protein regions, where phosphorylation often occurs, but where conventional binding domains have difficulty achieving specificity due to the absence of structured binding pockets. These challenges underscore the need for a fundamentally new approach to develop small, robust, and sequence-specific phospho-binders that can function inside living cells and serve as precision tools for sensing or modulating phosphorylation dynamics.

Deep learning based design of proteins has revolutionized the ability to create binders to challenging protein targets, but general methods for designing binders to covalently modified proteins and peptides have not been described. We reasoned that RoseTTAFold Diffusion2 (RFD2), a recently developed method for enzyme and small molecule binder design, could be generalized to designing binders for phosphotyrosine-containing (pY) peptides by training jointly on complexes of proteins with other proteins, small molecules, and with covalently modified proteins and peptides. We set out to extend RFD2 for binder design against this full range of targets and to explore the use of the new method for designing binders to pY containing peptides.

## RESULTS

### Designing binders to covalently modified proteins using RoseTTAFold Diffusion 2 for molecular interfaces (RFD2-MI)

RFD2 extended the backbone-level RFdiffusion framework to enable generation of proteins making specific sidechain-small molecule interactions using a flow-matching denoising objective (8, 9). RFD2 can design proteins with precise small-molecule binding sites for enzymes, using unindexed and tip-atom constraints to position catalytic groups at full atomic resolution without pre-specifying sequence placement. These capabilities make it highly effective for active-site scaffolding, but they are tailored to enzyme-ligand contexts. To enable binder design for protein-protein interactions or protein-ligand interfaces with defined binding sites and steerable interface properties we trained a new model based on RFD2 called RFD2 for molecular interfaces (RFD2-MI). We include additional interface examples and inject specialized 1D features that allow us to conditionally modify both the binder structure and the corresponding

binding site on the target. The 1D feature tensor in RFD2-MI is provided as a per token embedding (tokens are residues or atoms) that can encode amino-acid identity (one-hot), secondary-structure tokens (helix/strand/coil), motif flags, hotspot/antihotspot masks, solvent-accessibility, and any user-supplied conditions. At each diffusion step, RFD2-MI concatenates a per-residue 1D feature vector and then broadcasts that embedding to all of the residue's atom slots, so every coordinate update is conditioned on those features (**Figure 1A**).

RFD2-MI was trained on a curated, interface-focused dataset enriched for compact, well-packed binders in contact with their targets, while discarding poorly folded examples and trimming disordered or non-interacting regions for the binder (peptide targets are not trimmed). Hotspot and anti-hotspot masks guide interface geometry and prioritize key contacts. Binder placement is steered by the origin (ORI) of the starting residue Gaussian noise cloud, with optimal positioning achieved by centering it on the hotspot mask or near the intended binding site, yielding robust and shape-complementary designs (see Methods for details on training).

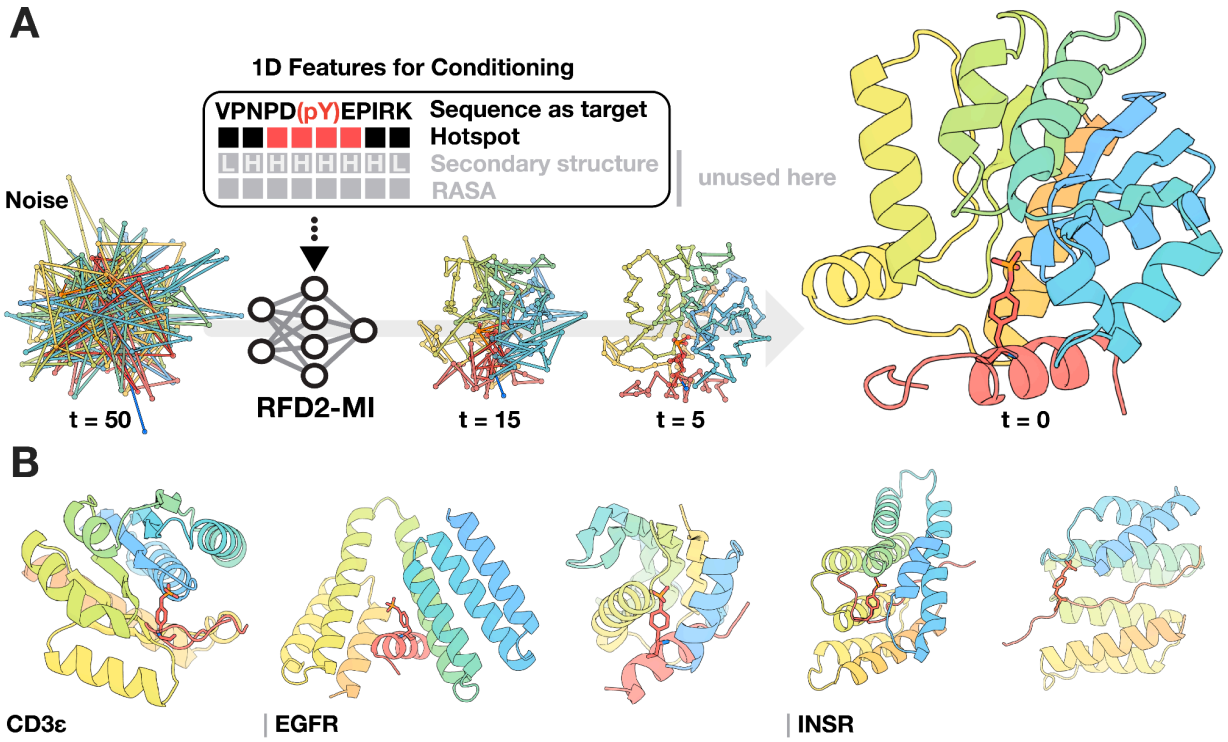


**Figure 1. RFD2-MI enables *de novo* design of phosphotyrosine-specific peptide binders from target sequence alone. (A)** Schematic of the RFD2-MI workflow. **(top)** The 1D conditioning feature channels can include hotspot/anti-hotspot masks, setting secondary structure, and solvent accessibility (RASA); in the examples shown here we design for a given peptide sequence, specified by sequence alone and conditioning on a hotspot mask (grayed items unused). Conditioning steers the model to form a pocket that positions the phosphotyrosine (pY; red/orange sticks in the peptide) and shapes complementary contacts in the designed binder (rainbow cartoon). **(bottom)** At each denoising step, the coordinates are diffused from noise (timesteps shown: t = 50, 15, 5, 0) while the binding site is guided through

1D conditioning features that are concatenated to the residue/atom embeddings. **(B)** Representative design outcomes for the three targets studied in this paper. RFD2-MI generated compact binders that cradle the cognate pY-containing peptide for CD3ε, EGFR, and INSR (coupled with the *Logos* pipeline). In all cases the phosphorylated residue (red/orange, shown as sticks) is coordinated by a pocket in the *de novo* binder (rainbow), while neighboring sequence-specific contacts help encode selectivity.

**Computational design and characterization of phosphorylation-specific binders**

We used RFD2-MI (**Figure 1A, B**) to design binders to phosphopeptide targets central to cellular signaling: 1) CD3ε, a component of the T-cell receptor, 2) two sites on epidermal growth factor receptor (EGFR), a potent oncogene, and 3) insulin receptor (INSR), a regulator of glucose metabolism dysregulated in diabetes. Because these phosphorylations take place within unstructured regions, we co-diffuse the designed protein and the target peptide, allowing the peptide to explore conformations that align with complementary binding pockets in the designed protein. In the case of INSR, we coupled this pipeline with the previously published Logos (12) method to integrate an interface for the disordered substrate (see Methods). Following structure generation, LigandMPNN was used to optimize the sequence for high affinity binding to the modified peptides. Designs were filtered based on the change in Gibbs free energy (ΔΔG) computed using Rosetta (10) for overall binding, the number of hydrogen bonds between the side chains of target and designed protein (for sequence specificity), and the number of hydrogen bonds between designed protein and phosphate (for phosphorylation specificity). For the INSR binders, we utilized the Logos pipeline (11, 12) to generate binders for adjacent non-modified regions in the target, and then used RFD2-MI to extend these to bind the full target including the pY modified region (see Methods for details). Designs for which AF3 predictions of the binder-target complex were close to the generated backbones after Rosetta FastRelax and for which the sidechain phosphate hydrogen bonds were recapitulated were selected for experimental validation.

We obtained synthetic DNA encoding 459 designs for CD3ε pY188, 5,082 designs for EGFR pY1068, 2,408 designs for EGFR pY1173, and 80 designs for INSR pY1361 (the latter generated with the Logos pipeline). For the CD3ε and EGFR binders, we displayed the designed proteins on yeast, and evaluated binding to both pY and unmodified targets. To do this, we incubated the yeast libraries with biotinylated non-phosphorylated peptides and streptavidin-Allophycocyanin (APC, far-red color), washed several times, incubated with excess biotin to block unbound Streptavidin-APC, and then incubated with biotinylated phosphorylated peptides and streptavidin-phycoerythrin (PE, red color). Designs specifically binding the phosphorylated target after several rounds of sorting were identified by sequencing. For the INSR binders, we obtained the individual genes encoding the designs and identified binders through direct *in vitro* purification and binding assays (see Methods for details).

For CD3ε, phosphorylation-dependent binders were identified by Sanger sequencing of 47 single clones grown from competition sort three (see Methods for more information). The sequences were closely related and one was cloned into plasmid pET29b+ for expression in E. coli. The identified expressed hit for CD3ε Y188 was assessed using biolayer interferometry

(BLI) and found to have a Kd of 1.5 μM to the phosphorylated CD3ε Y188 peptide target and undetectable binding for the non-phosphorylated version of the peptide (**Figure 2A-C, top**).

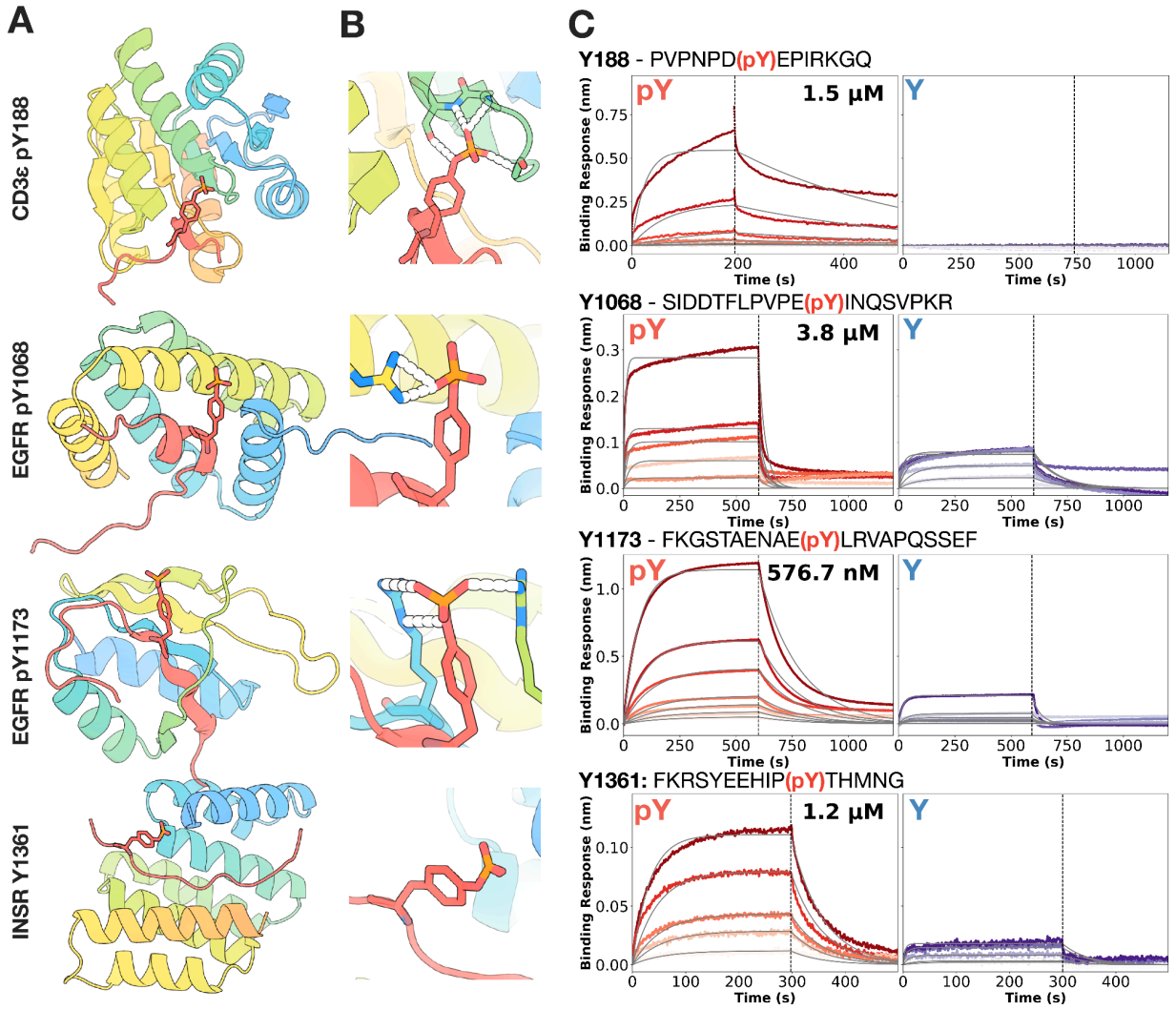


**Figure 2. Structural and biophysical characterization of phosphopeptide-specific binders. (A)** Design models (rainbow) for the four target peptides: CD3ε pY188 (top), EGFR pY1068 (second from top), EGFR pY1173 (second from bottom), and INSR (bottom). In each case the phosphorylated peptide (red/orange sticks) docks into the designed pocket with high correspondence between observed and predicted backbone and side-chain geometry. **(B)** Close-up views of key hydrogen-bonding networks (dashed lines) in the predicted complexes for CD3ε pY188 and EGFR pY1068 and INSR Y1361, highlighting how the phosphotyrosine moiety (red/orange sticks) is anchored by a conserved polar pocket in the binder (rainbow). **(C)** Representative biolayer interferometry (BLI) sensorgrams showing association and dissociation of each binder to phosphorylated (blue) versus non-phosphorylated (red) peptides, with global 1:1 kinetic fits overlaid in black. CD3ε pY188, EGFR pY1068, EGFR pY1173, INSR pY1361

exhibit dose-dependent binding only to the phosphorylated peptide, showing a much more obvious binding toward pY peptides than their unmodified counterparts.

For EGFR pY1068, 5,082 designs were obtained, 127 designs were identified to bind via yeast display, and the top 14 designs were selected for individual purification. Biolayer interferometry (BLI) showed that 7 designs bound to both phosphorylated and non-phosphorylated targets while 1 design bound preferentially to the phosphorylated form with a Kd of 3.8 μM (**Figure 2A-C, middle**). For EGFR pY1173, 2,408 designs were obtained, 87 designs identified via yeast display, and the top 10 designs individually purified. BLI showed that 6 designs bound to both phosphorylated and non-phosphorylated targets while 2 designs bound preferentially to the phosphorylated form with Kds as low as 577nM (**Figure 2A-C, middle**). For INSR, 71/80 total tested designs expressed solubly; 5/80 designs bound to both the phosphorylated and non-phosphorylated peptide. 2/80 designs bound considerably more strongly to phosphorylated peptide (Kd of 1.2 μM) than the non-phosphorylated version (**Figure 2C, bottom**).

For the phosphorylation-specific binders to CD3ε pY188 and EGFR pY1068, the phosphopeptide conforms partially to an α-helix with the phosphate at the end of the α-helix and the phosphate interacts with a loop region in the binder. In some instances (e.g CD3ε pY188 binder), designs coordinates the target phosphate group with the backbone atoms of a p-loop at the terminus of a helix, similar but not identical to the Walker motif (13, 14) associated with phosphate binding and coordination of ATP. For the phosphorylation-specific binders to EGFR pY1173, the phosphopeptide adopts a beta strand that pairs with a beta sheet in the binder; the phosphate is in the middle of the β-sheet, and the phosphate interacts with the side chains of residues in the neighboring β-sheets (**Figure 2A-B, middle**). For the Logos-derived INSR designs, the target has an extended confirmation and makes extensive polar interactions with the binder particularly around the charged phosphate group (**Figure 2B, bottom**), which likely confers the bias towards the phosphorylated version of the target.

**Structural validation of phosphorylation-specific binders**

The crystal structures of both the CD3ε pY188 and EGFR pY1068 binder-target complexes showed strong agreement with the design models (**Figure 3**). For the CD3ε pY188 complex, the overall complex Cα RMSD between the crystal structure and the design model is 2.1 Å, indicating the accuracy of the design methods. The phosphotyrosine was very accurately placed; following the superposition of the crystal structure and design model based on the binder, the RMSD on the phosphotyrosine was only 1.91 Å, demonstrating the capabilities of the model to design well coordinated phosphate binding motifs. For the EGFR pY1068 complex, structural agreement was also quite high, with a complex Cα RMSD of 2.2 Å relative to the design model. The phosphate in the model aligns well with the crystal structure, with an RMSD of 2.4 Å, indicating highly precise phosphorylated residue placement during design. The phosphate-binding pocket retained all intended hydrogen-bonding interactions, with the phosphate coordinated by two arginine side chains and the backbone amide of a nearby alanine residue. The relative orientation of the peptide and binder was essentially unchanged, and the local geometry around the phosphate group was reproduced with sub-angstrom accuracy. Taken together, these results highlight the accuracy of RFD2-MI-guided design in capturing not

only the global fold of the binder-target complex but also the precise positioning of phosphate-binding motifs.

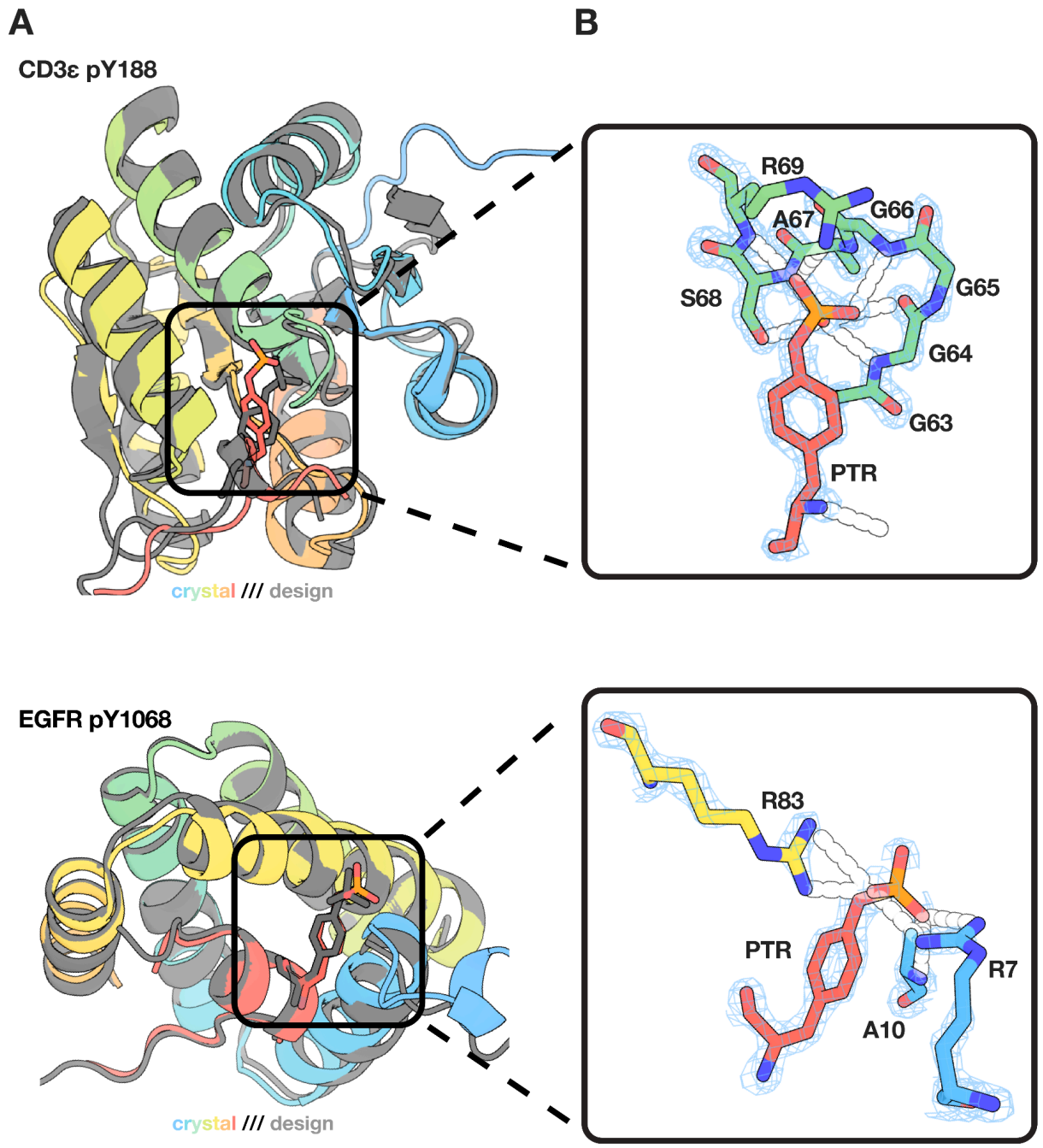


**Figure 3. Crystal structures of phosphorylation-specific binders match the design models. (A)** Overlays of the solved crystal structures (rainbow) with design models (gray) for CD3ε pY188 (top) and EGFR pY1068 (bottom). Black boxes indicate the binding pockets. The experimental structures closely follow the design models. **(B)** Zoomed views of the phosphate-recognition motifs with electron density shown as blue mesh. The phosphotyrosine (PTR) is displayed in sticks and contacting binder residues are labeled. For CD3ε pY188, a

short p-loop-like segment (G63-A67) coordinates the phosphate, capped by R69. For EGFR pY1068, the phosphate is chelated by two arginines (R7, R83) and stabilized by the nearby backbone amide of A10, illustrating the intended polar pocket that underlies phosphorylation specificity.

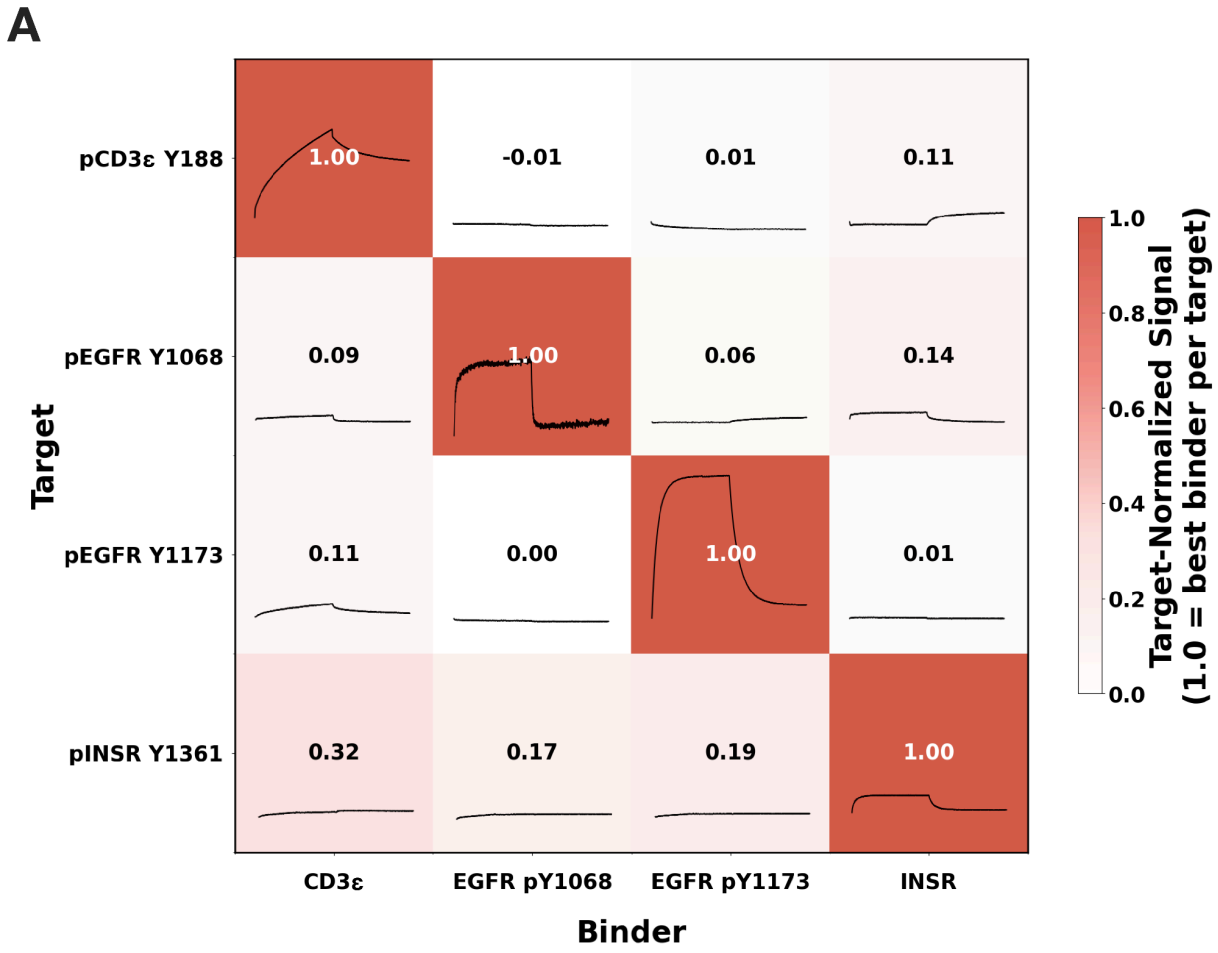


**Figure 4. Designed binders have sequence specificity. (A)** All-by-all binding heatmap displaying bio-layer interferometry (BLI) binding traces and normalized signal intensities. Phosphobinders (x-axis) were tested against target phosphopeptides (y-axis), with embedded kinetic traces showing association and dissociation profiles at the highest tested concentration. Color intensity and numerical values represent binding strength normalized to the strongest interaction per row (1.00 = 100% of maximum signal per target peptide). The matrix reveals specificity patterns, with strongest signals along the diagonal indicating preferential binding of each phosphobinder to its cognate target, while off-diagonal interactions demonstrate negligible cross-reactivity levels.

**Evaluation of sequence specificity**

With many phosphorylations occurring in a cell at any given time, differentiating between different phosphorylation sites is critical to understanding biological mechanisms. Ideally, our designed binders should be both phosphorylation and sequence specific to differentiate

phosphorylation sites. We encoded sequence specificity in our design pipeline in several ways. Structural sampling of both the designed protein and peptide target during RFD2-MI enables the designed protein to create a binding pocket for a particular peptide conformation, thus maximizing interactions. In addition, filtering for designs with multiple hydrogen bonds between the side chains of the design and target boosts the probability for sequence specificity as side chain-side chain interactions are sequence specific. Indeed, the designed pTYR peptide binders make extensive polar interactions with their target, which we anticipated would lead to sequence specificity. We assessed sequence specificity using an all-by-all BLI assay (**Figure 4**), measuring binding of four designs against each of the four targets against all four phosphopeptides. Strong signals were observed only for the cognate design-peptide pairs, with negligible signal for non-cognate pairs. These results demonstrate that the designs have sequence specificity.

## DISCUSSION

By introducing conditioning features in RFD2 geared towards designing molecular interactions and the implementation of PTM-aware modeling, we enabled the model to generate binders that precisely recognize phosphorylated targets. This enhanced model, called RFD2-MI, successfully generated compact and diverse binders to multiple phosphopeptides. The two crystal structures of designs in complex with their targets illustrate the accuracy of the design approach, which is notable given the challenges in binding the highly charged phosphate group. In contrast to previous affinity reagents such as antibodies, our *de novo* designs are not confined to a particular structural scaffold (12, 15); although RFD2-MI was trained on the PDB, the current model does not simply recapitulate designs with phospho-binding motifs like SH2 or 14-3-3 domains. This may be particularly useful when designing specific binders against phosphopeptide targets that do not have sequence similarity with phosphopeptides bound by natural proteins. More generally, the ability of RFD2-MI to generate binders to proteins, small molecules, and covalently modified proteins with state of the art performance makes it applicable to a very broad class of binder design problems.

While RFD2-MI has demonstrated success in designing binders to phosphotyrosines, there is room for improvement in our computational design pipeline as the success rate is low (often <0.1%) and the affinities of the best binders are modest (above 500nM). Overall, the challenge of achieving specificity for the phosphorylated versus unphosphorylated peptide was greater than the challenge of achieving sequence specificity: we obtained many designs that bound both phosphorylated and non-phosphorylated forms, while all phosphorylation-specific binders were also sequence-specific. This is not surprising given the challenge in binding the highly charged and solvated phosphate group–to achieve increased affinity with the phosphate present requires more than compensating for the lost interactions with solvent upon binding. The relatively low affinities of the best binders likely derive in part from the cost of phosphate desolvation; the two crystal structures show that the designs are quite accurate structurally. Future phosphopeptide design could benefit from greater focus on optimizing the interactions with the phosphate, while reducing slightly the emphasis on neighboring sequence contacts.

More generally, incorporation of multi-modal training data such as chemical, structural, and dynamic information (16) could further improve binder selectivity and functionality.

Our RFD2-MI approach can be readily generalized to other PTMs such as methylation, acetylation, or glycosylation to enable the generation of custom binders for a wide range of regulatory protein states previously considered undruggable (17, 18). These binders could enable researchers to build precise tools for detecting and manipulating individual sub-steps within signaling cascades, such as ligand engagement, adaptor recruitment, kinase activation, or effector binding. By targeting these discrete events, it should become possible to map signaling dynamics with higher resolution and uncover previously hidden regulatory checkpoints; such capabilities would not only improve our ability to sense and perturb signaling in living cells but also open new strategies for therapeutic intervention. Ultimately, our approach could transform how protein modifications are studied and exploited across biology and medicine.

## METHODS

### All-atom molecular interaction model training

RFD2-MI extends RFD2 to all-atom generative modeling of molecular interfaces between proteins and ligands. RFD2-MI uses the SE(3) flow matching architecture established in RFD2, with Gaussian probability paths for translations and Riemannian flow for rotations, to iteratively denoise heavy-atom coordinates and adds per token 1-D features for adding conditioning to get molecular interactions of choice and additional cropping strategies for training training examples.

RFD2-MI was trained with data sampling probabilities biased toward protein-protein complexes to 53% in order to enrich interface examples (19). Complex-like datasets were filtered to enforce a maximum binder length of 170 residues to control memory usage and match downstream cropping behavior. Folding quality was enforced via side-chain neighbor (SCN) analysis, where each binder residue's packing density was measured using a virtual Cβ cone and Cα neighbors. Two folding metrics were computed: binder_FBSCN (fraction of all binder residues with SCN > 4.0) and interface_FBSCN (same fraction but restricted to binder interface residues). Examples were rejected if binder_FBSCN < 0.12, interface_FBSCN < 0.13, or no hotspots were detected. To further improve physical plausibility, disordered N/C-terminal binder tails were trimmed using a 9-residue sliding window tolerance scheme, allowing removal of floppy segments even into hotspot regions if necessary. These steps, combined with a radial crop around hotspots, produced a dataset biased toward compact, interface-packed binders with well-structured interfaces, while excluding unfolded or non-contacting complexes for the binder. The targets are not assessed for packing and also not trimmed so peptide targets will stay intact for training purposes

To design binders against a target surface, we diffused only the binder while keeping the target fixed, conditioning on interface cues derived from hotspots and antihotspots on the target. A

target residue was labeled as a hotspot if its Cβ lay within 7 Å of any binder Cβ and its solvent-accessible surface area was at least 30 Å² (probe radius 2.8 Å). Hotspots were present in 75% of training examples and downsampled to at most 20% coverage using a speckle-or-region masking strategy, with optional floating-point "hotspot values" representing the local density of neighbors within 10 Å to emphasize high-contact "super-hotspots." Antihotspots were target residues more than 10 Å from any binder residue and were included in 10% of examples to discourage spurious contacts. Super hotspots augment the binary hotspot mask with a continuous weight per residue that reflects local contact density: for each hotspot that passes the 7 Å Cβ-Cβ proximity and 30 Å² SASA gate, we count cross-chain Cα neighbors within 10 Å, add small jitter (±1), cap at 12, and normalize to [0,1]. During training, a subset of hotspots are written to the numeric hotspot_values channel (instead of the boolean mask), so residues with the densest 10 Å cross-chain contacts receive values near 1 and are emphasized more strongly. This preserves the discrete hotspot definition while providing graded "super hotspot" strength to steer designs toward tightly packed interface cores.

To limit context while preserving local geometry, we radially cropped the target around a randomly selected binder hotspot, retaining residues within >25 Å of that hotspot (binder residues were always retained). Unstructured binder termini outside the interface were automatically trimmed using a sliding 9-residue window to measure side-chain neighbor support (sc_neigh threshold = 1.0). Terminal segments were removed if they contained ≤0/1/2 folded residues for windows of length ≤4/≤8/>8, respectively. If intervening residues between the cropped region and the hotspot bounds remained unfolded, trimming was permitted to extend slightly into the hotspot region. This procedure focused the model on compact, physically plausible binder-target interfaces while avoiding irrelevant or disordered regions. During training, the diffusion noise is centered at the origin (ORI), and the model learns correlation between the binder's center of mass and the center of that noise cloud. At inference we exploit this by choosing the ORI location to steer where the binder is placed (specified by a pseudoatom in the inference inputs). Placing ORI at the geometric center of the hotspot mask yielded the most consistent interface placement, though positioning it near the anticipated binder site also produced robust, shape-complementary designs.

In total three models were trained using different strategies. One model was fine-tuning from RF2 structure prediction weights (ppi_robust_struct) and two from pre-trained RFD2 weights: RFD_45 (ptm_finetuned) and RFD_140 (ppi_robust). Training examples for ppi_robust and ppi_robust_struct were filtered for well folded structures as described above. ptm_fintuned was trained with additional examples of phosphorylation binding motifs from the pdb that were previously excluded during training with additional focus on masking target coordinates in some examples. This allows to generate both binder structure and target conformation at the same time, similar as in RFDiffusion (https://github.com/RosettaCommons/RFdiffusion/blob/main/examples/design_ppi_flexible_peptide.sh) and Liu et al. (20).

**Binder design and prediction**

Protein binders targeting a specific phosphopeptide sequence were computationally designed using a multi-stage protocol. Initial binder scaffold generation was performed with RFdiffusion

(using the AA_ppi model where applicable), constraining the binder length to fewer than 160 amino acids. During this process, the target phosphopeptide sequence was held fixed, while its coordinates were allowed to co-diffuse with the *de novo* binder backbone. Following backbone generation, binder sequences were designed using LigandMPNN. For generated backbones that include a predefined structured motif (i.e., short peptide-protein interface coordinate) generated from Logos on a 4-7 amino acid peptide side, the key motif residues were held fixed during this sequence design step. The resulting protein-peptide complex structures were refined using the Rosetta FastRelax protocol, followed by a subsequent round of LigandMPNN to optimize the sequence for the relaxed structure. At this stage, an initial filtering step was applied to remove any design that did not form at least two hydrogen bonds with the phosphate group of the target phosphotyrosine residue. Finally, the structures of promising binder-peptide complexes were predicted using AlphaFold3 resulting in the final design model.

**Iterative sequence diversification**

To expand the pool of potential candidates, AlphaFold3 predictions that passed the filtering criteria (detailed below) were subjected to an additional round of sequence design. The predicted backbone conformations of the binder-peptide pairs were held rigid, and LigandMPNN was utilized to generate sequence variants for the binder scaffold. This iterative technique aimed to increase sequence diversity for promising backbones. The newly generated sequences were then re-submitted for AlphaFold3 structure prediction and subsequently evaluated against the established filtering metrics.

**Design filtering criteria**

Predicted binder-peptide structures from AlphaFold3 were rigorously filtered based on a combination of model confidence metrics and specific structural features. Designs were retained only if they met the following criteria:

1. Model Confidence: High per-residue confidence for the binder (high pLDDT), low inter-domain predicted aligned error between the binder and peptide (low iPAE), high inter-domain predicted TM-score (high iPTM), and a high overall predicted TM-score for the binder (high PTM).
2. Binding Specificity: To ensure focused interaction with the phosphotyrosine, designs were required to have at least two hydrogen bonds to the phosphotyrosine's phosphate group. To penalize non-specific or excessive non-phosphorylated binding, designs with more than twelve total hydrogen bonds to the peptide were excluded.
3. Motif Fidelity: For designs built around a structural motif, the root-mean-square deviation (RMSD) of the phosphotyrosine residue between the designed and predicted structures was required to be less than 5 Å. This criterion ensures the target residue remains correctly oriented within the intended binding pocket.

In our experience, successful designs had a low iPAE between the binder and the phospho-residue of the peptide, and a high pLDDT for the target phospho-peptide, which is indicative of a highly confident prediction for the binding mode. In filtering sequence-backbone pairs we also took inspiration from the fact that several known phospho-binding motifs form

extensive hydrogen bond networks to the phosphate group (e.g. SH2 domains), and as expected the crystal structures match the AF3 prediction of the designed sequence (21, 22).

**DNA library preparation**

Sequences were padded with a (GGGS)n linker at the C terminal of designs to avoid biased amplification of short PCR fragments during PCR. Selected binder protein sequences were reverse translated using DNAworks2.0 for optimal expression in *S.cerevisae.* Oligo pools for the *de novo* binders were ordered from Twist Bioscience. Pools were amplified with Kapa HiFI Polymerase (Kapa Biosystems) using a qPCR machine (BioRAD CFX96). FIrst, pools were amplified in a 25 uL reaction and terminated at half the maximum yield, avoiding over-amplification. PCR product was then loaded onto a DNA agarose gel, excised, and extracted with QIAquick Clean Up Kit (Qiagen, Inc.). 2-3 micrograms of pETCON vector and 6 micrograms of amplified DNA was transformed into yeast.

**Peptide synthesis**

Protected phospho amino acids (e.g. Fmoc-Tyr(PO(OBzl)OH)-OH) were purchased from Millepore Sigma. Phosphopeptides were synthesized on a 0.1mmol scale via microwave-assisted solid-phase peptide synthesis (SPPS) using a CEM LibertyBlue peptide synthesizer and standard SPPS protocols. Peptides were subsequently coupled with Fmoc-AHX-OH (P3 Biosystems, 3eq.), HATU (Millepore Sigma, 3eq.), and N,N-dimethylformamide (DIEA, Millepore Sigma, 5eq) in DMF for 3 hours, then treated with 20% piperidine (Millepore Sigma) in DMF for 2 x 15 min, washed thoroughly with DMF and swelled with 50/50 DMSO/DMF for 30m prior to coupling with D-Biotin (Millepore Sigma, 3eq), HATU (3eq), DIEA (5eq) in 50/50 DMSO/DMF for 3 hours. The labeled peptide was then globally deprotected with a cleavage cocktail of 92.5/2.5/2.5/2.5 TFA/TIPS/H2O/2,2-(ethhylenedioxy)diethanetihol for 3h, concentrated briefly *in vacuo*, and precipitated into ice cold diethyl ether. The crude peptide was washed with ether and dried under nitrogen, then was resuspended in a minimal amount of water and acetonitrile (ACN) and purified via RP-HPLC (A: H2O with 0.1% TFA, B: ACN with 0.1% TFA) in a linear gradient from 5%B to 45%B. Fractions were collected and analyzed for product using an Agilent G6230B TOF, then pooled and lyophilized to yield pure phosphopeptide.

**Yeast surface display**

A yeast surface display library was constructed using S. cerevisiae strain EBY100 transformed with a plasmid pool encoding the binder variants. Initial cultures were grown overnight at 30 °C in a selective synthetic complete medium lacking tryptophan and uracil (C-Trp-Ura), supplemented with 2% (w/v) glucose. For protein expression, the culture was diluted 1:10 into SGCAA auto-induction medium containing 0.2% (w/v) glucose and incubated overnight at 30 °C. Following induction, cells were washed with chilled PBS supplemented with 1% (w/v) Bovine Serum Albumin (PBSF). To confirm and enrich for clones expressing the binder construct, an initial sort was performed. Cells were labeled with a fluorescein isothiocyanate (FITC)-conjugated anti-c-Myc antibody (Miltenyi Biotec), which targets a c-Myc epitope tag on the displayed protein. The FITC-positive population was collected via FACS and regrown to generate an enriched expression library for subsequent affinity-based sorting.

Cells were regrown and washed, then labelled with biotinylated target (peptide) using two techniques - with avidity and without avidity. With avidity labeling, cells were incubated with biotinylated target, anti-c-Myc fluoresceinisothiocyanate (FITC, Miltenyi Biotech), and streptavidin-phycoerythrin (SAPE, ThermoFisher). Concentration of SAPE with the avidity method was 1/4 of the biotinylated target concentration. After the first few rounds of screening using the with-avidity method, weak binder candidates were eliminated. Using the without-avidity method, cells were incubated with a biotinylated target, washed, and then incubated with SAPE and FITC. Subsequent sorts were applied with varying concentrations.

**Competition-based sorting for phosphopeptide specificity**

In some instances, to isolate binders with high specificity for the phosphorylated peptide, a competitive sorting strategy was employed. The induced and washed yeast library was first incubated with 300 nM of a biotinylated, unphosphorylated "decoy" peptide. Following a wash step, free biotin was added to the cell suspension to quench any unbound streptavidin-conjugated reagents and minimize non-specific interactions in the subsequent step. Next, cells were incubated with 100 nM of the biotinylated phosphopeptide "target." To detect binding, the unphosphorylated peptide was labeled with an anti-biotin antibody conjugated to Allophycocyanin (APC), while the phosphopeptide was labeled with an anti-biotin antibody conjugated to Streptavidin-Phycoerythrin (SAPE). Using FACS, distinct cell populations were gated and sorted;

1. Specific Binders: High SAPE signal and low/negative APC signal.
2. Non-specific Binders: High APC signal.
3. Dual-Recognition Binders: High signal in both SAPE and APC channels.

Populations showing specific binding to the phosphopeptide were collected, regrown, and subjected to up to three additional rounds of sorting to achieve high enrichment.

**Isolation and Sanger sequencing of individual clones**

The enriched cell population from the final sorting round was plated on solid agar medium for yeast growth and incubated overnight at 30°C. Individual colonies were isolated, and the plasmid DNA was prepared for amplification via colony PCR. A small portion of each colony was boiled to lyse the cells, and the binder-encoding DNA insert was amplified using vector-specific primers (pETCON primers). PCR products of the expected size were purified and analyzed by Sanger sequencing to determine the DNA sequence of individual high-performing protein binders.

**Next-generation sequencing (NGS) of enriched populations**

To comprehensively analyze the convergence of the selected binder pool, an aliquot of the sorted cells from each round of enrichment was collected for NGS analysis. Plasmid DNA was extracted from the bulk sorted populations using a commercial extraction kit (Zymoprep, Zymo Research). The variable binder-encoding regions were then amplified from the extracted plasmid pool via PCR using primers that both flanked the insert and appended Illumina-compatible sequencing adapters and indices. The resulting amplicon libraries were purified, quantified, and sequenced on an Illumina platform (NextSeq/MiSeq). This deep

sequencing approach allowed for the quantitative tracking of sequence diversity and the enrichment of specific binder families throughout the selection campaign.

**Bacterial protein production and purification**

*E. coli* Lemo21(DE3) strains were transformed with the pET29b+ plasmid encoding the binder gene. Cells were then grown for 24 hours in liquid broth medium supplemented with kanamycin and inoculated at 1:50 mL ratio in the Studier TBM-5052 autoinduction medium supplemented with kanamycin for several hours at 37°C, then grown overnight at 18°C. Cells were collected by centrifugation at 4,000 g at 4°C for 15 min, resuspended in 30 mL of lysis buffer (20 mM Tris-HCl, pH 8.0, 300 mM NaCl, 30 mM imidazole, 1 mM PMSF and 0.02 mg ml-1
DNase). The cell resuspension was lysed by sonication for 2.5 min (5 second cycles) and the lysate was clarified by centrifugation at 24,000 g at 4°C for 20 min. The supernatant was passed through a Ni-NTA nickel resin, pre-equilibriated with a wash buffer (20 mM Tris-HCl, pH 8.0, 300 mM NaCl and 30 mM imidazole). The resin was washed twice with 10 column volumes of wash buffer and eluted with 3 column volumes of elution buffer (wash buffer with 300 mM imidazole). Eluted proteins were concentrated using Ultra-15 Centrifugal Filter Units and purified with Superdex 75 Increase 10/300 GL size exclusion column in TBS (25 mM Tris-HCl, pH 8.0, and 150 mM NaCl). Fractions containing monomeric proteins were pooled, concentrated and snap-frozen.

**Direct production of proteins from designs (23)**

Linear gene fragments encoding the binder design sequences were cloned into the LM627 vector using Golden Gate assembly. These subcloning reactions were performed in 96-well PCR plates with a 4 µL reaction volume. Following this, 1 µL of the reaction mixture was transformed into chemically competent E. coli BL21 (DE3) cells. After a 1-hour recovery period in 100 µL of SOC medium, the transformed cell suspensions were transferred directly into a 96-deep well plate containing 900 µL of LB media supplemented with Kanamycin. After overnight incubation at 37°C, 100 µL of the growth culture was inoculated into 96-deep well plates containing 900 µL of auto-induction media (autoclaved TBII media with Kanamycin, 2 mM $MgSO_4$, 1X 5052). The cultures were then expressed overnight at room temperature. Cells were harvested by centrifugation at 4000 x g for 15 minutes. The bacterial pellets were lysed in 100 µL of lysis buffer (1X BugBuster (Millipore #70921-4), 0.01 mg/mL DNase, 1 Pierce protease inhibitor tablet per 50 mL lysis) for 30 minutes on shaker, 220 RPM. The lysates were spun down by centrifugation at 4000 x g for 10 minutes, followed by purification using Ni-charged MagBeads (GenScript #L00295). The wash buffer contained 25 mM Tris pH 8.0, 300 mM NaCl, and 10 mM Imidazole, while the elution buffer contained 25 mM Tris pH 8.0, 300 mM NaCl, and 500 mM Imidazole. 250 µL of wash buffer was used to wash twice while 120 µL of elution buffer was used to collect eluted proteins. Filtered elutions were then submitted to HPLC, S200. For samples showing major monomeric peaks, protein concentrations were determined by measuring absorbance at 280 nm with a NanoDrop spectrophotometer (Thermo Scientific), using extinction coefficients and molecular weights calculated from their amino acid sequences.

**Biolayer interferometry**

Protein-peptide interactions were measured using an Octet RED96 System (ForteBio) with streptavidin-coated biosensors (ForteBio). Wells containing 200 uL of solution, and HBS-EP+ buffer (GE Healthcare Life Sciences, 10 mM HEPES pH 7.4, 150 mM NaCl, 3 mM EDTA, 0.05% (v/v) surfactant P20) plus 1% non-fat dry milk blotting grade blocker (BioRad). Biosensor tips were loaded with target peptide at 5μM for 300 s (threshold of 0.6 nm response), then incubated in the HBS-EP+ buffer for 60s for baseline measurement. Tips were then dipped into the solution containing binder for 600s (association) and finally, dipped into the HSP-EP+ buffer for 600s (dissociation). Binding data was analyzed with ForteBio Data Analysis Software version 9.0.0.10.

**Protein crystallography and structure determination**

Purified protein was used for crystallization trials using the sitting drop vapor diffusion method. Crystallization trials were set up by Mosquito LCP from SPT Labtech. Formulated total 200 nL drops using the 96-well plate format at 20˚C. Crystal search was conducted on plates using UV imaging (UVEX microscopes and UVEX PS-256 from JAN Scientific). Diffraction quality crystals were obtained with the following conditions;

1. CD3ε-pY188 crystals grew in 2.0 M Sodium chloride and 10% (w/v) PEG 6000.
2. EGFR-pY1068 crystals grew in 0.1 M Na HEPES pH 7.0 and 2 M ammonium sulfate

Diffraction data was obtained either at the National Synchrotron Light Source II on beamline 17_ID-1 (AMX) or Advanced Photon Source on beamline NECAT 24ID-E. XDS was used to integrate x-ray intensities and subsequent data reduction (24). Data was merged and scaled using Pointless/Aimless in the CCP4 program suite (25). Molecular replacement (Phaser program) was used for structure determination and phasing (26). Models were improved using Phenix autobuild (rebuild-in-place set to false, using simulated annealing (27)). Manual model building was performed using COOT (28). The final model was evaluated using MolProbity (29).

## Author Contributions

Conceptualization and overall study design: A.L., A.M., B.C., D.B., D.T., F.D., G.R.L., H.R.A.T., J.Z.Z., K.W., M.S.B., P.S., R.K., W.A.; Contribution of code and ideas: B.C., D.J., D.T., H.R.A.T., M.S.B., P.S., R.I.B., R.K., W.A., J.Y.; Model training and optimization: B.C., D.T., G.R.L., H.R.A.T., J.Y., M.S.B., W.A.; Pipeline development for phosphopeptide binder design: G.R.L., I.K., J.Z.Z., K.A.K., K.W., M.S.B.; Computational binder design and structural analysis: G.R.L., J.S., J.Z.Z., K.A.K., K.W., L.H., M.S.B., R.K.S., S.Z.; Peptide synthesis and reagent preparation: C.M., X.L.; Yeast library construction: D.K.V., N.R.; Yeast display screening and selection: G.R.L., J.S., J.Z.Z., K.A.K., M.S.B., R.K.S., S.Z.; Protein expression and purification: G.R.L., J.Z.Z., K.A.K., K.W., M.S.B.; Biophysical characterization: G.R.L., J.S., J.Z.Z., K.A.K., M.S.B.; Crystallization, data collection, and structural determination: A.K., A.K.B., E.J.; Supervision and project administration: D.B., F.D., J.Z.Z., L.S., M.S.B.; Writing - original draft and review & editing: B.C., D.B., G.R.L., J.Z.Z., K.A.K., K.W., M.S.B., with input from all authors.

## Competing Interests

The authors declare no competing interests.

## Code and Data Availability

All code and data will be made available upon final publication.

## Acknowledgements

We thank L. Goldschmidt and K. VanWormer and their teams for maintaining the computational and wet lab resources at the Institute for Protein Design.

We gratefully acknowledge support from the Bill and Melinda Gates Foundation (INV-043758), the Defense Threat Reduction Agency (HDTRA1-19-1-0003, HDTRA1-21-1-0038), and a gift from Microsoft. This work was further supported by the Helmsley Charitable Trust Type 1 Diabetes Program (2019PG-T1D026), the Howard Hughes Medical Institute, and the Human Frontiers Science Program (RGP0061/2019).

We thank Spark Therapeutics for support through the project *Computational Design of a Half Size Functional ABCA4*. We also acknowledge the Audacious Project at the Institute for Protein Design, the Open Philanthropy Project Improving Protein Design Fund, and the Open Philanthropy Project Universal Flu Vaccine Fund.

This material is based upon work supported by the National Science Foundation (CHE-2226466). Additional support came from the National Institutes of Health, including the

National Cancer Institute (R01CA240339, K99 CA293001), the National Institute of Allergy and Infectious Diseases (R01AI160052, 1U19AI181881-01), and the National Institute on Aging (R01AG063845).

This work was delivered in part as part of the Matchmakers team supported by the Cancer Grand Challenges partnership funded by Cancer Research UK (CGCATF-2023/100008) and the National Cancer Institute (OT2CA297288-01). We also acknowledge support from the Advanced Research Projects Agency for Health (APECx Program, 1AY1AX000036), and the Washington Research Foundation Innovation Fellows Program.

## Funding Sources

This work was supported in part by the Advanced Research Projects Agency for Health (ARPA-H APECx); the Audacious Project (Audacious Discretionary Sub, Audacious Hub, Audacious Project at IPD Consortium); the Bill & Melinda Gates Foundation (BMGF 2, Structure-Based Design); Cancer Research UK (Cancer Grand Challenges, CGC); the Defense Advanced Research Projects Agency (DARPA Catalytic Sponge); the Defense Threat Reduction Agency (DTRA MACROCYCLES, DTRA J5B_ML-MACROCYCLES, DTRA J5C_FORCEFIELD-ML); the Department of Energy (Principles of De Novo); the Fred Hutchinson Cancer Center (C19 HHMI Initiative [SAGE-CYCLE-C94170]); the Institute for Protein Design Enzyme Design Fund; the International Human Frontier Science Program Organization (UCLA HFSP); Merck Sharp & Dohme Corp. (Merck Upfront); Merck Sharp & Dohme LLC (Baker_Merck_Project01); Microsoft (Protein Prediction Research); the National Cancer Institute (BAKER_NKC, K99 CA293001); the National Institute of Allergy and Infectious Diseases (U19 NIAID ReVAMPP); the National Institutes of Health (BAKER_BBB, C19 NIH R01 Minibinder, R01 Protein Structure); the National Science Foundation (NSF MFB); Northwestern University (DTRA NU ML DOMANE); Novo Nordisk A/S (CDA_Novo Nordisk 3); the Open Philanthropy Project (IPD Improving Protein, IPD Universal Flu Vaccine); Spark Therapeutics, Inc. (SPARK); the Leona M. and Harry B. Helmsley Charitable Trust (Helmsley Diabetes); Thermo Fisher Scientific Inc. (DiMaio Thermo Fisher); and the Washington Research Foundation (Fund Innovation in Protein Design).

## REFERENCES


1. S. Mazhar, D. Leonard, A. Sosa, D. Schlatzer, D. Thomas, G. Narla, Challenges and Reinterpretation of Antibody-Based Research on Phosphorylation of Tyr307 on PP2Ac. *Cell Rep.* 30, 3164-3170.e3 (2020).
2. D. Li, Y. K. Cho, High specificity of widely used phospho-tau antibodies validated using a quantitative whole-cell based assay. *J. Neurochem.* 152, 122–135 (2020).
3. H. A. Lashuel, A.-L. Mahul-Mellier, S. Novello, R. N. Hegde, Y. Jasiqi, M. F. Altay, S. Donzelli, S. M. DeGuire, R. Burai, P. Magalhães, A. Chiki, J. Ricci, M. Boussouf, A. Sadek, E. Stoops, C. Iseli, N. Guex, Revisiting the specificity and ability of phospho-S129 antibodies to capture alpha-synuclein biochemical and pathological diversity. *npj Park.'s Dis.* 8, 136 (2022).
4. T. Kaneko, H. Huang, X. Cao, X. Li, C. Li, C. Voss, S. S. Sidhu, S. S. C. Li, Superbinder SH2 Domains Act as Antagonists of Cell Signaling. *Sci. Signal.* 5, ra68 (2012).
5. G. Veggiani, H. Huang, B. P. Yates, J. Tong, T. Kaneko, R. Joshi, S. S. C. Li, M. F. Moran, G. Gish, S. S. Sidhu, Engineered SH2 domains with tailored specificities and enhanced affinities for phosphoproteome analysis. *Protein Sci.* 28, 403–413 (2019).
6. G. D. Martyn, G. Veggiani, U. Kusebauch, S. R. Morrone, B. P. Yates, A. U. Singer, J. Tong, N. Manczyk, G. Gish, Z. Sun, I. Kurinov, F. Sicheri, M. F. Moran, R. L. Moritz, S. S. Sidhu, Engineered SH2 Domains for Targeted Phosphoproteomics. *ACS Chem. Biol.* 17, 1472–1484 (2022).
7. H. Liu, H. Huang, C. Voss, T. Kaneko, W. T. Qin, S. Sidhu, S. S.-C. Li, Surface Loops in a Single SH2 Domain Are Capable of Encoding the Spectrum of Specificity of the SH2 Family*[S]. *Mol. Cell. Proteom.* 18, 372–382 (2019).
8. W. Ahern, J. Yim, D. Tischer, S. Salike, S. M. Woodbury, D. Kim, I. Kalvet, Y. Kipnis, B. Coventry, H. R. Altae-Tran, M. Bauer, R. Barzilay, T. S. Jaakkola, R. Krishna, D. Baker, Atom level enzyme active site scaffolding using RFdiffusion2. *bioRxiv*, 2025.04.09.648075 (2025).
9. J. Yim, A. Campbell, A. Y. K. Foong, M. Gastegger, J. Jiménez-Luna, S. Lewis, V. G. Satorras, B. S. Veeling, R. Barzilay, T. Jaakkola, F. Noé, Fast protein backbone generation with SE(3) flow matching. *arXiv*, doi: 10.48550/arxiv.2310.05297 (2023).
10. E. H. Kellogg, A. Leaver-Fay, D. Baker, Role of conformational sampling in computing mutation-induced changes in protein structure and stability. *Proteins: Struct., Funct., Bioinform.* 79, 830–838 (2011).
11. K. Wu, H. Bai, Y.-T. Chang, R. Redler, K. E. McNally, W. Sheffler, T. J. Brunette, D. R. Hicks, T. E. Morgan, T. J. Stevens, A. Broerman, I. Goreshnik, M. DeWitt, C. M. Chow, Y. Shen, L. Stewart, E. Derivery, D. A. Silva, G. Bhabha, D. C. Ekiert, D. Baker, De novo design of modular peptide-binding proteins by superhelical matching. *Nature* 616, 581–589 (2023).
12. K. Wu, H. Jiang, D. R. Hicks, C. Liu, E. Muratspahić, T. A. Ramelot, Y. Liu, K. McNally, S. Kenny, A. Mihut, A. Gaur, B. Coventry, W. Chen, A. K. Bera, A. Kang, S. Gerben, M. Y.-L. Lamb, A. Murray, X. Li, M. A. Kennedy, W. Yang, Z. Song, G. Schober, S. M. Brierley, J. O'Neill, M. H. Gelb, G. T. Montelione, E. Derivery, D. Baker, Design of intrinsically disordered region binding proteins. *Science* 389, eadr8063 (2025).
13. M. L. R. Romero, F. Yang, Y.-R. Lin, A. Toth-Petroczy, I. N. Berezovsky, A. Goncearenco, W. Yang, A. Wellner, F. Kumar-Deshmukh, M. Sharon, D. Baker, G. Varani, D. S. Tawfik, Simple yet functional phosphate-loop proteins. *Proc. Natl. Acad. Sci.* 115, E11943–E11950 (2018).

14. J. E. Walker, M. Saraste, M. J. Runswick, N. J. Gay, Distantly related sequences in the alpha- and beta-subunits of ATP synthase, myosin, kinases and other ATP-requiring enzymes and a common nucleotide binding fold. *EMBO J.* 1, 945–951 (1982).
15. J. Z. Zhang, X. Li, A. R. Batingana, C. Liu, H. Jiang, K. Shannon, B. J. Huang, K. Wu, D. Baker, De novo design of Ras isoform selective binders. bioRxiv, 2024.08.29.610300 (2025).
16. M. T. Degiacomi, Coupling Molecular Dynamics and Deep Learning to Mine Protein Conformational Space. *Structure* 27, 1034-1040.e3 (2019).
17. X. Xie, T. Yu, X. Li, N. Zhang, L. J. Foster, C. Peng, W. Huang, G. He, Recent advances in targeting the "undruggable" proteins: from drug discovery to clinical trials. *Signal Transduct. Target. Ther.* 8, 335 (2023).
18. L. E. Smith, A. Rogowska-Wrzesinska, The challenge of detecting modifications on proteins. *Essays Biochem.* 64, 135–153 (2020).
19. R. Krishna, J. Wang, W. Ahern, P. Sturmfels, P. Venkatesh, I. Kalvet, G. R. Lee, F. S. Morey-Burrows, I. Anishchenko, I. R. Humphreys, R. McHugh, D. Vafeados, X. Li, G. A. Sutherland, A. Hitchcock, C. N. Hunter, A. Kang, E. Brackenbrough, A. K. Bera, M. Baek, F. DiMaio, D. Baker, Generalized biomolecular modeling and design with RoseTTAFold All-Atom. Science 384, eadl2528 (2024).
20. C. Liu, K. Wu, H. Choi, H. Han, X. Zhang, J. L. Watson, S. Shijo, A. K. Bera, A. Kang, E. Brackenbrough, B. Coventry, D. R. Hick, A. N. Hoofnagle, P. Zhu, X. Li, J. Decarreau, S. R. Gerben, W. Yang, X. Wang, M. Lamp, A. Murray, M. Bauer, D. Baker, Diffusing protein binders to intrinsically disordered proteins. bioRxiv, 2024.07.16.603789 (2024).
21. T. Kaneko, R. Joshi, S. M. Feller, S. S. Li, Phosphotyrosine recognition domains: the typical, the atypical and the versatile. *Cell Commun. Signal.* 10, 32 (2012).
22. H. C. Reinhardt, M. B. Yaffe, Phospho-Ser/Thr-binding domains: navigating the cell cycle and DNA damage response. *Nat. Rev. Mol. Cell Biol.* 14, 563–580 (2013).
23. J. Qian, L. F. Milles, B. I. M. Wicky, A. Motmaen, X. Li, R. D. Kibler, L. Stewart, D. Baker, Accelerating protein design by scaling experimental characterization. bioRxiv, doi: 10.1101/2025.08.05.668824 (2025).
24. W. Kabsch, XDS. *Acta Crystallogr. Sect. D: Biol. Crystallogr.* 66, 125–132 (2010).
25. L. Potterton, J. Agirre, C. Ballard, K. Cowtan, E. Dodson, P. R. Evans, H. T. Jenkins, R. Keegan, E. Krissinel, K. Stevenson, A. Lebedev, S. J. McNicholas, R. A. Nicholls, M. Noble, N. S. Pannu, C. Roth, G. Sheldrick, P. Skubak, J. Turkenburg, V. Uski, F. von Delft, D. Waterman, K. Wilson, M. Winn, M. Wojdyr, CCP4i2: the new graphical user interface to the CCP4 program suite. *Acta Crystallogr. Sect. D: Struct. Biol.* 74, 68–84 (2018).
26. A. J. McCoy, R. W. Grosse-Kunstleve, P. D. Adams, M. D. Winn, L. C. Storoni, R. J. Read, Phaser crystallographic software. *J. Appl. Crystallogr.* 40, 658–674 (2007).
27. D. Liebschner, P. V. Afonine, M. L. Baker, G. Bunkóczi, V. B. Chen, T. I. Croll, B. Hintze, L.-W. Hung, S. Jain, A. J. McCoy, N. W. Moriarty, R. D. Oeffner, B. K. Poon, M. G. Prisant, R. J. Read, J. S. Richardson, D. C. Richardson, M. D. Sammito, O. V. Sobolev, D. H. Stockwell, T. C. Terwilliger, A. G. Urzhumtsev, L. L. Videau, C. J. Williams, P. D. Adams, Macromolecular structure determination using X-rays, neutrons and electrons: recent developments in Phenix. Acta Crystallogr. Sect. D 75, 861–877 (2019).
28. P. Emsley, K. Cowtan, Coot: model-building tools for molecular graphics. Acta Crystallogr. Sect. D: Biol. Crystallogr. 60, 2126–2132 (2004).

29. C. J. Williams, J. J. Headd, N. W. Moriarty, M. G. Prisant, L. L. Videau, L. N. Deis, V. Verma, D. A. Keedy, B. J. Hintze, V. B. Chen, S. Jain, S. M. Lewis, W. B. Arendall, J. Snoeyink, P. D. Adams, S. C. Lovell, J. S. Richardson, D. C. Richardson, MolProbity: More and better reference data for improved all-atom structure validation. Protein Sci. 27, 293–315 (2018).

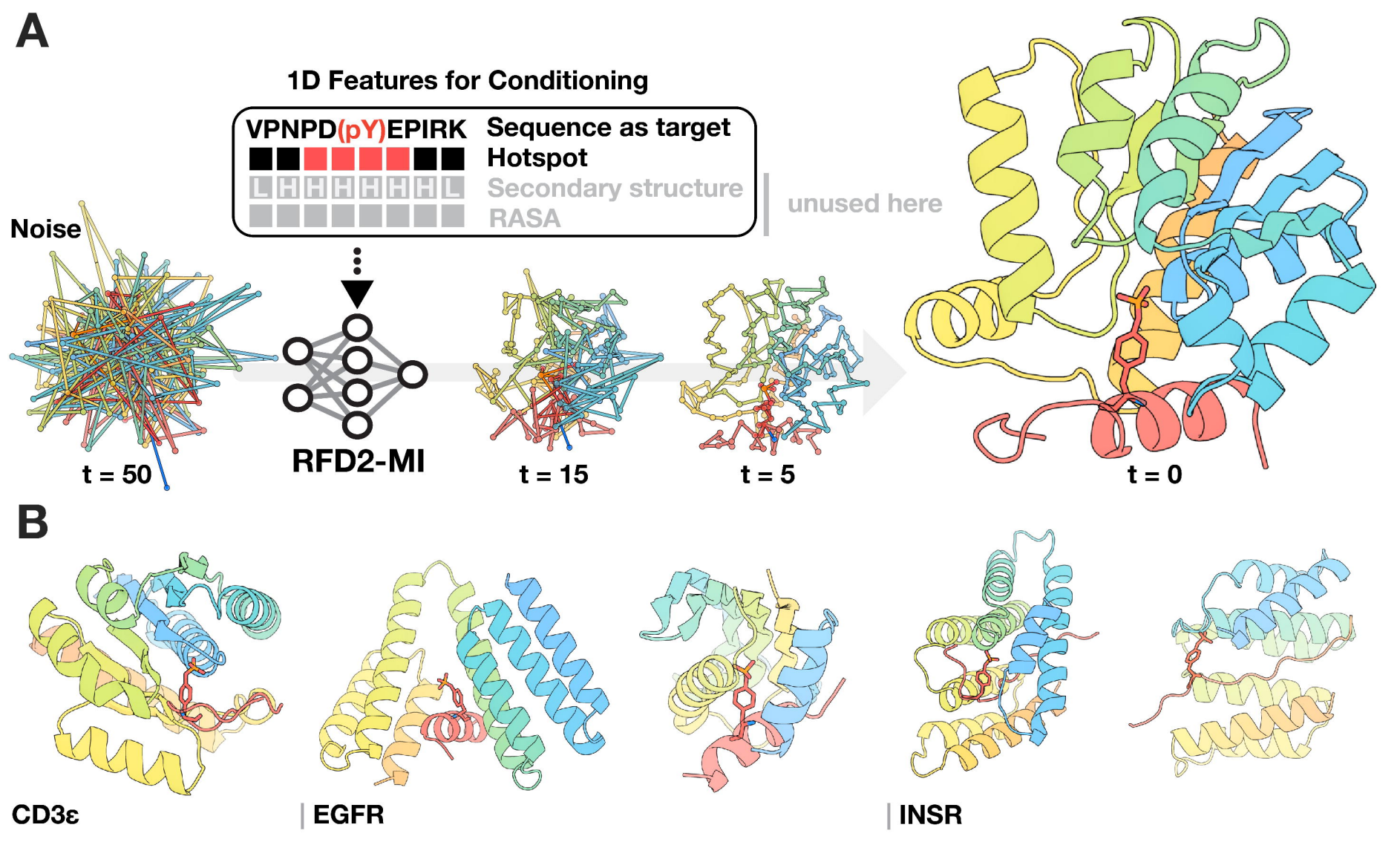
A
1D Features for Conditioning
VPNPD(pY)EPIRK
Sequence as target
Hotspot
L H H H H H H L
Secondary structure
RASA
unused here
Noise
RFD2-MI
t = 50
t = 15
t = 5
t = 0
B
CD3ε
EGFR
INSR

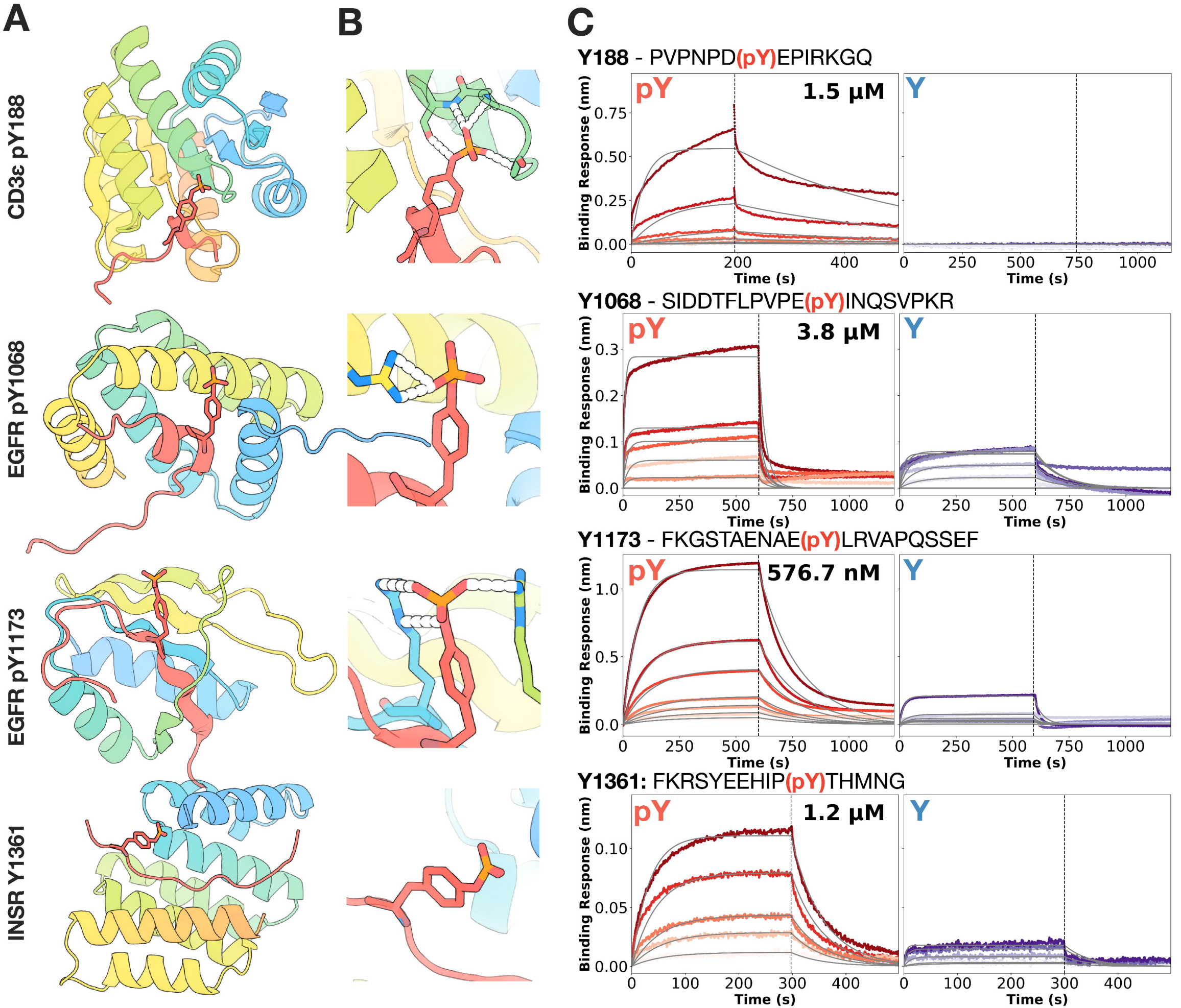
A
B
C
CD3ε pY188
EGFR pY1068
EGFR pY1173
INSR Y1361
Y188 - PVPNPD(pY)EPIRKGQ
pY
1.5 μM
Y
Y1068 - SIDDTFLPVPE(pY)INQSVPKR
pY
3.8 μM
Y
Y1173 - FKGSTAENAE(pY)LRVAPQSSEF
pY
576.7 nM
Y
Y1361: FKRSYEEHIP(pY)THMNG
pY
1.2 μM
Y
Binding Response (nm)
Time (s)

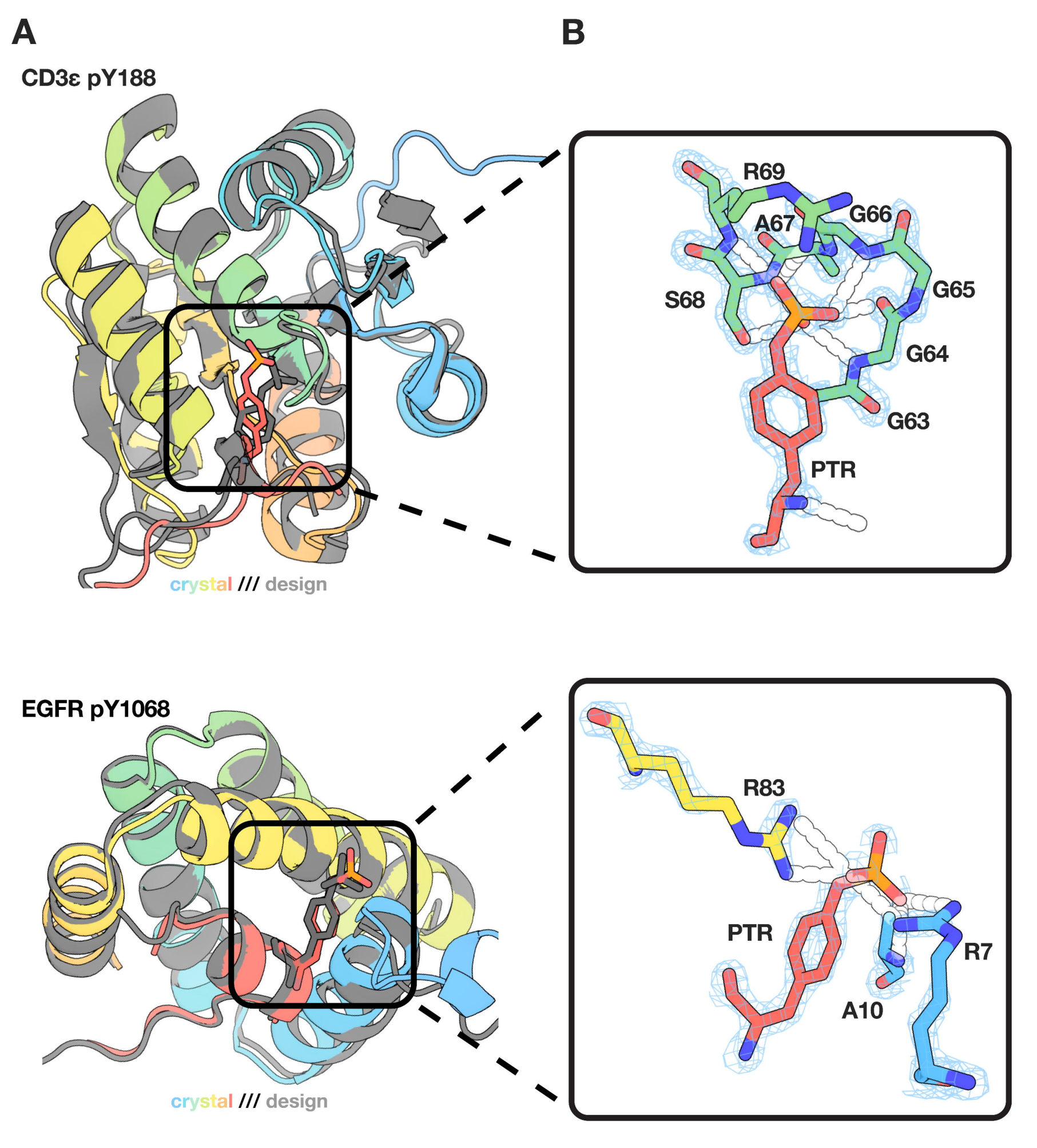
A
B
CD3ε pY188
R69
A67
G66
S68
G65
G64
G63
PTR
crystal /// design
EGFR pY1068
R83
PTR
R7
A10
crystal /// design

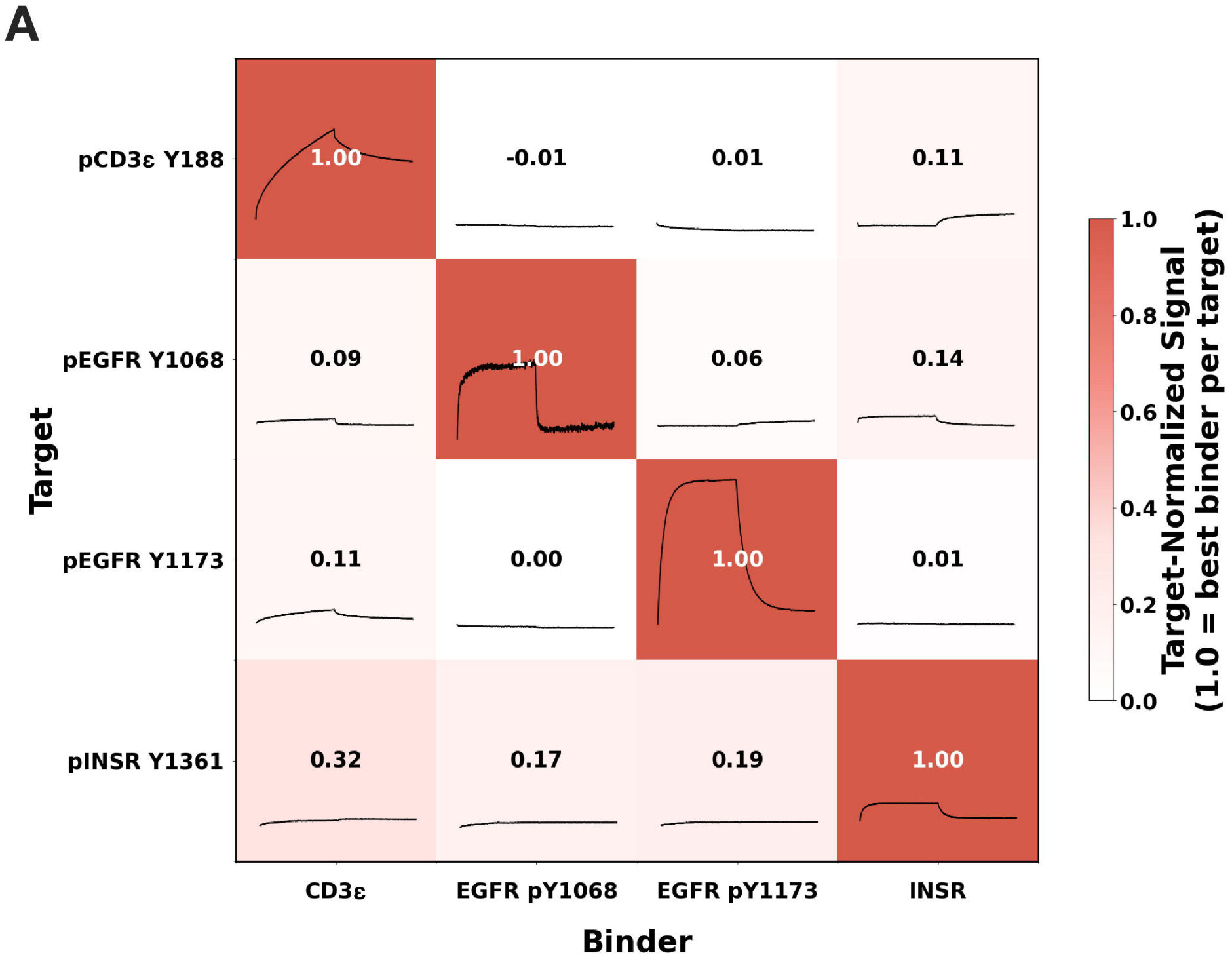
A
pCD3ε Y188
pEGFR Y1068
pEGFR Y1173
pINSR Y1361
Target
1.00
-0.01
0.01
0.11
0.09
1.00
0.06
0.14
0.11
0.00
1.00
0.01
0.32
0.17
0.19
1.00
CD3ε
EGFR pY1068
EGFR pY1173
INSR
Binder
1.0
0.8
0.6
0.4
0.2
0.0
Target-Normalized Signal
(1.0 = best binder per target)